Desalination and Water Treatment
www.deswater.com
doi: 10.5004/dwt.2023.30185

316 (2023) 185–197
December

Adsorptive removal of methyl orange from aqueous solution by hydrotalcite derived catalysts

Nadia Aider[a,d,*], Baya Djebarri[b,d], Fouzia Touahra[c,d,*], Djamila Halliche[d]

[a]*Laboratoire de Chimie Appliquée et de Génie Chimique (LCAGC), Université Mouloud Mammeri, 150 0 0, Tizi-Ouzou, Algeria, email: nadia.aider@ummto.dz*
[b]*Laboratory of Applied Chemistry and Materials (LabCAM), University of M'hamed Bougara of Boumerdes, Avenue de l'Indépendance Boumerdes, 35000 Algeria, email: b.djebarri@univ-boumerdes.dz*
[c]*Centre de Recherche Scientifique et Technique en Analyses Physico-chimiques (CRAPC), BP 384-Bou-Ismail, RP42004, Tipaza, Algeria, email: tfafaze256@yahoo.fr*
[d]*Laboratory of Natural Gas Chemistry, Faculty of Chemistry (USTHB), BP, 32, 16111, Algiers, Algeria, email: dhalliche@yahoo.fr*

Received 16 August 2023; Accepted 19 November 2023

ABSTRACT

The objective of our work is to study the adsorption of methyl orange dye over $ZnAl_2O_4$ and ZnO-$ZnAl_2O_4$ derived from hydrotalcite in order to highlight their potential as low-cost adsorbents for the treatment of water. The materials $ZnAl_2$, Zn_2Al were synthesized *via* co-precipitation method and were characterized using various characterization techniques, which showed that the obtained materials corresponds to the compounds of hydrotalcite. Different parameters were studied to optimize the process of methyl orange removal on samples derived from hydrotalcite, including the mass of the adsorbent, the contact time, the concentration, and pH. On the other hand, adsorption isotherms were studied using Langmuir and Freundlich models, as well as the effect of these solids on thermodynamic quantities. According to the results obtained, the ZnO-$ZnAl_2O_4$ has the greatest adsorption capacity compared to the $ZnAl_2O_4$. The interaction of these materials with the dye shows that the adsorption kinetics are fast and follows a second-order adsorption rate expression. The maximum adsorption capacity determined by the Langmuir mathematical model is about 62.85 mg/g for ZnO-$ZnAl_2O_4$ and 46.24 mg/g for $ZnAl_2O_4$ and the thermodynamic study led to the conclusion that the adsorption is endothermic and that the adsorption process is spontaneous.

Keywords: Adsorption isotherms; ZnO-$ZnAl_2O_4$; Hydrotalcite; Methyl orange; Co-precipitation

1. Introduction

In recent decades, scientists, governments and civil society have become aware of the threat of environmental pollution which can endanger all kinds of lives [1,2]. This threat not only poses human health problems, but also has dangerous toxicological impacts on the environment [3]. Water pollution, linked to human activity, generally consists of industrial discharges, in particular the textile industry uses synthetic dyes [4]. The presence of these dyes in water is harmful even at the low doses and the increase in its concentration leads to massive mortality of species, but they also have less visible effects: eutrophication of the environment [5].

There are several conventional processes applied in wastewater decontamination such as biological treatments [6], physico-chemical processes and adsorption [6–8]. These methods have proven effective but in most cases very expensive.

* Corresponding author.

In this study, we opted for the adsorption process which is considered as one of the promising methods which satisfy all the qualities of a fundamental technology that we are looking to forward to the wastewater treatments [9]. In this sense, research focuses on the development of new materials with effective and selective properties of adsorption or catalytic degradation of these pollutants.

The double lamellar hydroxides (LDHs) also known as anionic clays or hydrotalcite compounds [10]. Hydrotalcite materials are quite rare in nature but relatively required and simple to synthesize in the laboratory [10,11]. These materials have functional properties associated with specific structural properties, their ability to trap negatively charged species by surface adsorption or anion exchange thanks to their positive surface charge and the flexibility of the interlayer reflect their potential applications as ion exchangers, catalysts or catalyst carriers, adsorbents for removing pollutants from solutions [12]. The general formula of hydrotalcite can be expressed as follows: $[M^{2+}_{1-x}M^{3+}_{x}(OH)_2][A^{n-}]_{x/n}, yH_2O$, where M^{2+} and M^{3+} are di- and trivalent metal cations in the octahedral positions of brucite-like layers and A^{n-} is an interlayer anion. Several research studies have investigated the adsorption of methyl orange (MO) on different types of hydrotalcite. However, they have done little work on the adsorption of MO by ZnAl hydrotalcite. Investigations carried out by Machrouhi et al. [13] showed that highest adsorption capacity of patent blue V dye by Zn/Al hydroxide occurred and calcined forms at acidic medium. Thus, the optimal conditions to achieve high equilibrium adsorption capacity were achieved at pH = 5, adsorbent dosage = 100 mg/L, and initial dye concentration = 15 mg/L by calcined ZnAl.

ZnAl-layered hydrotalcite synthesized by the urea method were efficiently utilized by El Khanchaoui et al. [14] for their photocatalytic activities for the removal of Congo red (CR) dye from water. They concluded that the amount of CR uptake onto hydrotalcite increases with increasing initial dye concentration and temperature from 25°C to 245°C.

The purpose of this paper is to study the effect of the mixed oxides ($ZnAl_2O_4$ and ZnO-$ZnAl_2O_4$) derived from their precursor ZnAl-hydrotalcite on adsorption of methyl orange (MO). The adsorbent properties of hydrotalcite compounds with respect to MO dye have been studied as well as the various parameters influencing adsorption such as the molar ratios (Zn^{2+}/Al^{3+} = 0.5 and 2), the mass of the material, the contact time, the concentration, and the temperature of the reaction medium. We have also developed some isotherms and kinetic models in order to better understand the adsorption mechanism of dye molecules.

2. Materials and methods

2.1. Materials

The necessary chemicals used in this study were of analytical grade such as methyl orange (MO), NaOH, HCl, $Zn(NO_3)_2{\cdot}6H_2O$ and $Al(NO_3)_3{\cdot}9H_2O$. These products were supplied by the chemical company Merck (Taufkirchen, Germany) and used without further purification. The physico-chemical properties of methyl orange (MO) are given in Table 1.

2.2. Preparation of the adsorbents

$ZnAl_2$ and Zn_2Al have been synthesized easily, according to the co-precipitation method described elsewhere [16] with two molar ratios (Zn/Al = 0.5 and 2). The aqueous solution of $Zn(NO_3)_2{\cdot}6H_2O$ and $Al(NO_3)_3{\cdot}9H_2O$ was added dropwise to a solution of NaOH (2 M) under stirring. Next, the gel obtained was aged at 100°C for 15 h with vigorous stirring. Finally, the product obtained was filtered and washed with distilled water, then dried and finely ground. The samples were calcined under air from room temperature up to 600°C in increments of 5°C/min and held for 5 h at the ultimate calcination temperature to produce the mixed oxides. The metal oxides obtained by calcining $ZnAl_2$ and Zn_2Al are respectively named: $ZnAl_2O_4$ and ZnO-$ZnAl_2O_4$.

2.3. Adsorption test

The adsorption of MO contained in aqueous solutions on the $ZnAl_2O_4$, and ZnO-$ZnAl_2O_4$ materials was investigated as an effect of adsorbent mass 50–300 mg, initial dye concentration 10–150 mg/L and temperature 25°C–70°C.

Equilibrium adsorption experiments were used to investigate methyl orange dye removal. During these experiments, 20 mL of MO solution at an initial concentration of dye fixed at 100 mg/L was placed in a 100 mL flasks containing 50 mg of the suspended sorbent. These flasks were placed in a reciprocating multi-position shaker with stirring at 250 rpm and at a constant temperature 25°C.

The effect of adsorbent mass, adsorbate concentration and temperature were studied respectively in the ranges of 50–300 mg, 10–150 mg/L and 25°C–70°C. We also examined the effect of solution pH on the adsorption capacity, series of MO solutions were prepared by adjusting the pH in a range of 2.0–12.0 using a solution of HCl or NaOH. After a previously fixed stirring time, the solution with the adsorbent is recovered and then filtered; the recovered filtrate is analyzed by visible UV Spectroscopy (Spectrophotometer PMC Milliot brand UVmini-1240) by measuring the absorbance at λ_{max}. The adsorption capacity of dye or amount of dye adsorbed (Q_t) presented in mg/g was determined by using Eq. (1) [17]:

$$Q_t = \frac{(C_0 - C_t)V}{m} \tag{1}$$

where C_0 and C_t are denoted as initial and equilibrium dye concentrations (mg/L), respectively, m is the mass of the adsorbent used (g) and V volume (L) of the solution.

Table 1
Physico-chemical properties of methyl orange [15]

Usual name	Methyl orange
Chemical formula	$C_{14}H_{14}N_3NaO_3S$
Molecular weight (g/mol)	327.33 g/mol
Solubility in water (g/L)	5 (20°C)
λ_{max} (nm)	438
pKa	3.5
Density (g/cm^3)	1.28
Melting point (°C)	300

2.4. Characterization of adsorbent

The chemical composition of each material was estimated using atomic absorption spectroscopy (AAS) with Varian SpectrAA 110 (Milton Freewater, Oregon, USA). The dissolution of solids was affected in the presence of nitric acid. The specific surface area of samples and pore size distribution calculations were determined by nitrogen adsorption using standard Brunauer–Emmett–Teller (BET) and Barrett–Joyner–Halenda methods. Adsorption isotherms of nitrogen at 77 K under study was recorded using a static volumetric apparatus ASAP 2020 (Micromeritics, Norcross, GA, USA). The structure of samples was confirmed by X-ray powder diffraction with a Seifert C-3000 diffractometer (Germany) with filtered CuKα (λ = 1.5418 Å). Fourier-transform infrared (FTIR) spectra were recorded on an ALPHA Bruker (single reflection diamond ATR) spectrometer in the region 400–4,000 cm^{-1}.

3. Results and discussion

3.1. Chemical analyses

The experimental molar ratios and the chemical formulas of the obtained products are shown in Table 2.

The results of the elemental analysis by AAS show that the molar ratios Zn^{2+}/Al^{3+} are in good agreement with those calculated, taking into account the initial salt concentration. This confirms the quantitative precipitation of the precursor salt.

3.2. X-ray diffraction analysis

The X-ray diffraction (XRD) spectra of the uncalcined samples are shown in Fig. 1a and b. These spectra essentially show a strong crystallinity of the framework of the hydrotalcite. XRD patterns for this type of materials showed several diffraction peaks [18].

- Sharp symmetrical diffraction peaks around 2θ = 11.65°, 23.43°, 35.3° corresponding respectively to the diffraction plane (003), (006), (012).
- Broad asymmetrical peaks corresponding to planes (015), (018), (110) and (113) are clearly distinguished between 37° and 75°. These two types of peaks constitute a kind of fingerprint of the formation of the crystalline structure of hydrotalcite [19]. Fig. 1a and b gather also the X-ray diffraction spectra obtained after calcination. It is known that the calcination of hydrotalcites leads to their dehydration ($-H_2O$) then to dihydroxylation ($-HO^-$) and decarboxylation ($-CO_3^{-2}$) which are accompanied by the collapse of the lamellar structure when the calcination temperature is high enough [18,20]. The X-ray diffraction spectra obtained after calcination shows, the disappearance of the diffraction lines characteristic of the hydrotalcite structure and appeared of the mixed oxides. The diffraction pattern of Zn_2Al calcined gives the ZnO (JCPDS 36-1451) predominantly phase and $ZnAl_2O_4$ spinel (JCPDS 12-0328) as a secondary phase. Thus, the X-ray diffraction spectra of the calcined $ZnAl_2$ shows the formation of the pure $ZnAl_2O_4$ spinel phase.

Table 2
Chemicals composition, proposed formulas and the Brunauer–Emmett–Teller surface for the prepared samples

Samples	Molar ratios $R=\left[\frac{nM^{2+}}{nM^{3+}}\right]=\left[\frac{(1-x)}{x}\right]$	Chemical formulas $\left[M^{2+}_{(1-x)}M^{3+}_{(1-x)}\right]$	S_{BET} (m^2/g)
$ZnAl_2$	0.53	$Zn_{0.35}Al_{0.65}$	67.79
$ZnAl_2O_4$	–	–	45.40
Zn_2Al	2.22	$Zn_{0.69}Al_{0.31}$	96.48
ZnO-$ZnAl_2O_4$	–	–	155.07

3.3. FTIR spectra analysis

The infrared spectra of uncalcined and calcined samples are represented in Fig. 2a and b. FTIR spectra for uncalcined samples show various absorption bands which are characteristics of hydrotalcite structure containing mainly carbonate anions. The broad band around 3,380 cm^{-1}, is attributed to the valence vibration of the hydroxyl groups of water molecules and the hydroxyl groups of the brucite layers. The absorption at 1,635 and 1,600 cm^{-1}, respectively

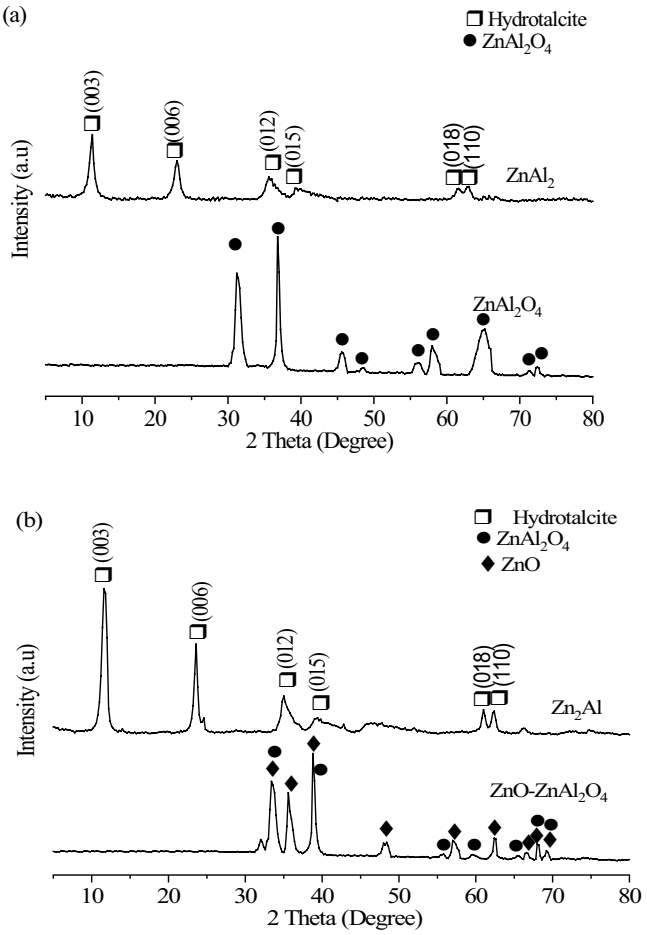

Fig. 1. X-ray diffraction patterns of (a) $ZnAl_2$, $ZnAl_2O_4$ and (b) Zn_2Al, ZnO-$ZnAl_2O_4$.

in the case of $ZnAl_2$ and Zn_2Al samples, corresponds to the O–H bending vibration of water molecules in the interlayer space, while the bands at 1,325–1,330 cm^{-1} characteristic of the $-CO_3^{2-}$ groups from carbon dioxide (CO_2) of the air.

The bands of base frequency vibration that appear below 1,000 cm^{-1} are due to metal-oxygen or oxygen-metal-oxygen bonds, so the bands at 715 and 750 cm^{-1} are attributed to valence vibration MO (Zn–O) [20]. FTIR spectra of the calcined samples at 600°C, are illustrated also in Fig. 2a and b. After calcination, trace amounts of the carbonate were found around 1,330 cm^{-1} formed from atmospheric carbon dioxide. A strong decrease of the peak located around 1,600 cm^{-1} is also observed. These changes are due to the loss of water molecules in the interlayers. Below 1,000 cm^{-1}, the absorption peaks of the Zn–O and/or Al–O stretching and bending vibration modes was observed. The result suggests the phase transformation of hydrotalcite into mixed oxides; which was in good agreement with the reported XRD pattern results (Fig. 1).

3.4. Scanning electron microscopy analysis

Scanning electron microscopy (SEM) images for uncalcined and calcined solids shown in Fig. 3. The SEM images of $ZnAl_2$ (Fig. 3a) and Zn_2Al samples (Fig. 3b), show irregular hexagonal platelet-like sheets; the hexagonal morphology typical of hydrotalcites. Similar results were observed by Yu et al. [21] for ZnAl-CO_3 and MgAl-CO_3 hydrotalcites.

However, $ZnAl_2O_4$ (Fig. 3c). and ZnO-$ZnAl_2O_4$ (Fig. 3d) show a mixture of irregular crystalline compared with the samples before calcination. The aggregated particles may be attributed to the mixed oxides due to the removal of water, nitrate and carbonate from the interlayer space of the hydrotalcite structures [21].

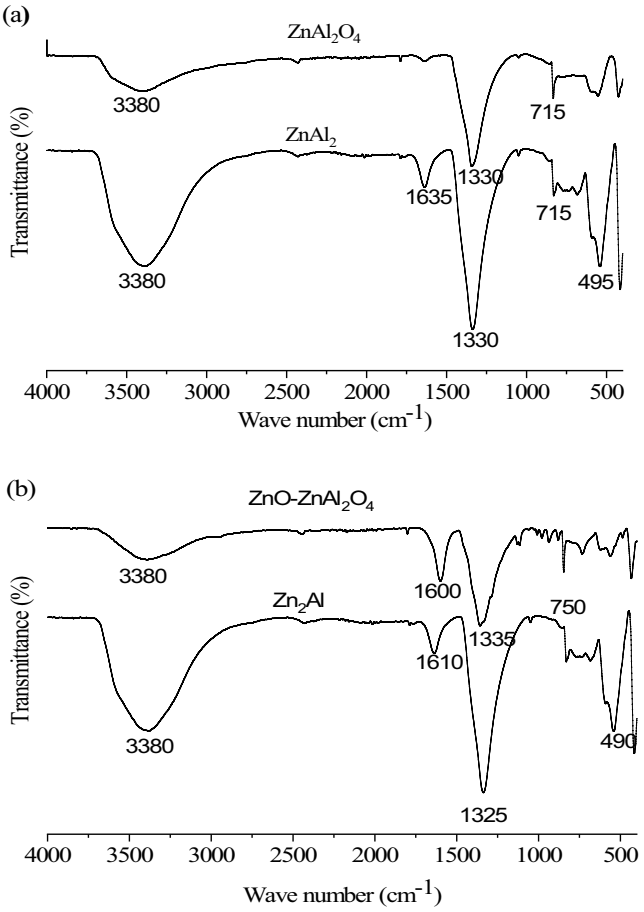

Fig. 2. Fourier-transform infrared spectra of (a) $ZnAl_2$, $ZnAl_2O_4$ and (b) Zn_2Al, ZnO-$ZnAl_2O_4$.

3.5. BET surface analysis

The nitrogen adsorption/desorption isotherms and the pore size distribution curves of the Zn_2Al, $ZnAl_2$, $ZnAl_2O_4$ and ZnO-$ZnAl_2O_4$ samples are given in Fig. 4. According to the International Union of Pure and Applied Chemistry (IUPAC classification), the Zn_2Al and $ZnAl_2$ samples exhibited a type IV isotherm with H1 hysteresis loop due to the typical layered structures of hydrotalcites. While the N_2 adsorption–desorption isotherms of $ZnAl_2O_4$ and ZnO-$ZnAl_2O_4$ samples exhibit type IV isotherms with the hysteresis type H3, which are typical of mesoporous and slit shaped materials character with a pore size that varies between 2 and 50 nm [21].

The results obtained (Table 2) show that the specific surface of Zn_2Al presents the highest surface area (96.48 m^2/g) compared to Zn_2Al (67.79 m^2/g). The specific surface area of the two samples increases after calcination at 600°C. This result can be explained by the fact that during the calcination step, the solids undergo degassing phenomena of H_2O and CO_3^{2-} (in the form of CO_2) that are found in the pores on the surface of the materials [22]. This phenomenon leads to a decrease in pore size and an increase in specific surface area.

3.6. pH of the zero point of charge pH_{pzc}

The pH at the point of zero charge (pH_{pzc}) of an adsorbent is an important parameter for characterizing the solid-solution interface, it corresponds to the pH for which the surface of the solid has zero charge.

The graph that represents the ΔpH as a function of the initial pH allows us to determine the pH_{pzc} which corresponds to ΔpH = 0, or final pH = initial pH (ΔpH = final pH – initial pH). According to Fig. 5, the pH_{pzc} of $ZnAl_2O_4$ and ZnO-$ZnAl_2O_4$ are respectively 6.1 and 7.2. For pH > pH_{pzc}, the surface is negatively charged, while for pH < pH_{pzc}, the surface is positively charged.

3.7. Adsorption of methyl orange on hydrotalcite

3.7.1. Effect of the pH

The pH of the solution is an important parameter that affects the dye adsorption process. It also modifies the surface charge of the adsorbent [23].

The effect of pH on the adsorption of MO by $ZnAl_2O_4$ and ZnO-$ZnAl_2O_4$ was investigated from pH 2 to 11, while keeping all other parameters constant. Fig. 6 represents the variation of adsorption quantities of MO in function of solution pH. It is clear that the performance of ZnO-$ZnAl_2O_4$ was better than $ZnAl_2O_4$ in the adsorption of MO

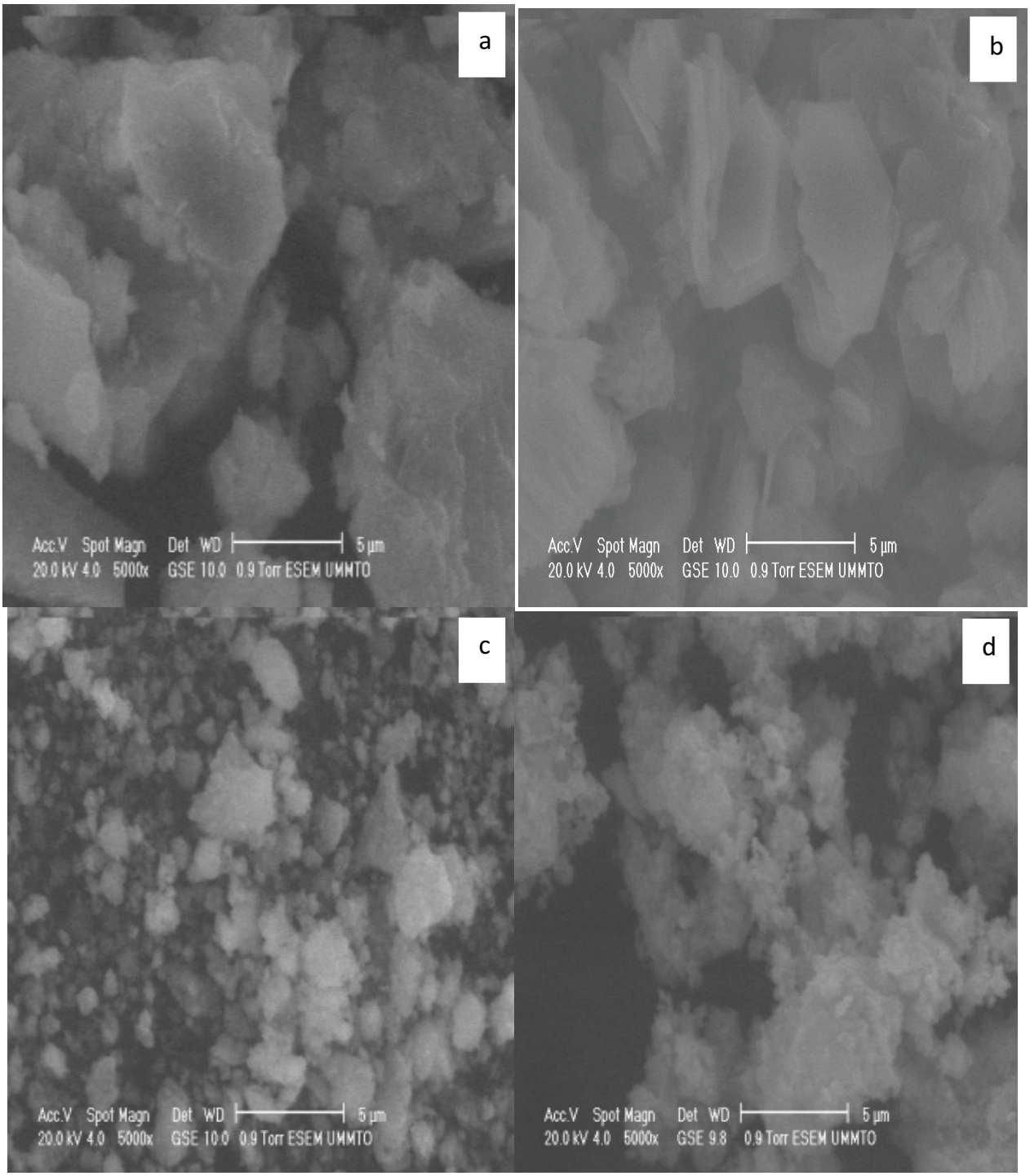

Fig. 3. Scanning electron microscopy images: (a) $ZnAl_2$, (b) Zn_2Al, (c) $ZnAl_2O_4$ and (d) ZnO-$ZnAl_2O_4$.

from the aqueous solution at different pH values studied. As depicted in Fig. 6, adsorption quantities of MO increased moderately to up to 44.5% at pH 6 for $ZnAl_2O_4$ and 52.2% at pH 7 for ZnO-$ZnAl_2O_4$. In an aqueous solution, MO molecules can lose a proton, leading to the formation of sulfonate group ($–SO_3^-$) ions. This deprotonation results in the MO molecule having a negative charge. In the meanwhile, the adsorbents ($ZnAl_2O_4$ and ZnO-$ZnAl_2O_4$), have a positive surface because the oxygen atoms on these materials are protonated. This positive surface generates electrostatic attraction between the negatively charged MO ions and the positively charged adsorbent surface, promoting adsorption [24]. However, the removal efficiency of MO decreases at pH levels between 7 and 11, this decrease can be attributed to the

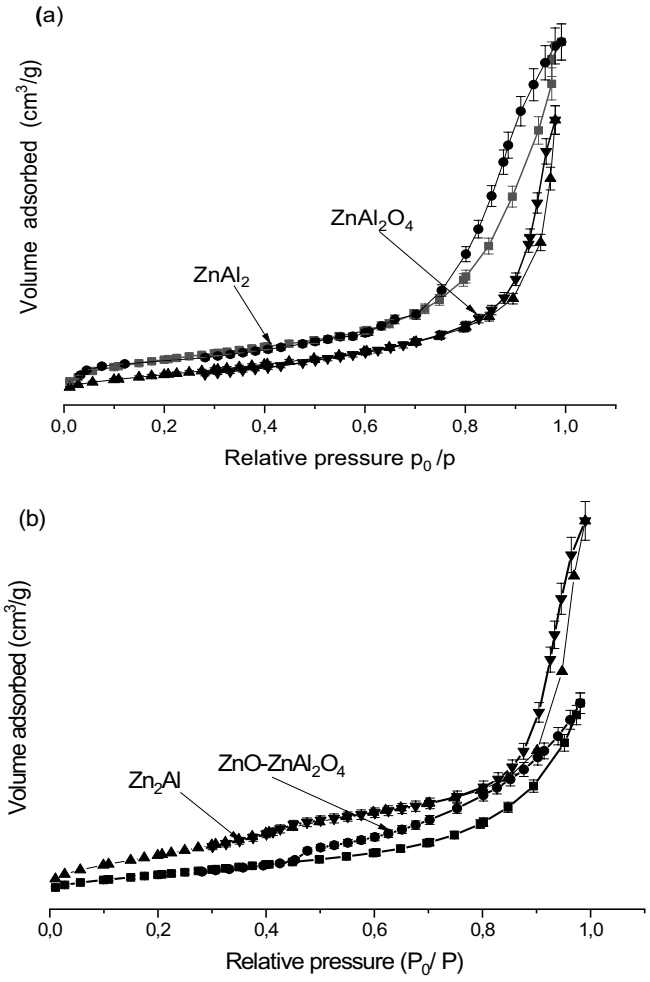

Fig. 4. Nitrogen sorption isotherms of (a) $ZnAl_2$, $ZnAl_2O_4$ and (b) Zn_2Al, $ZnO\text{-}ZnAl_2O_4$.

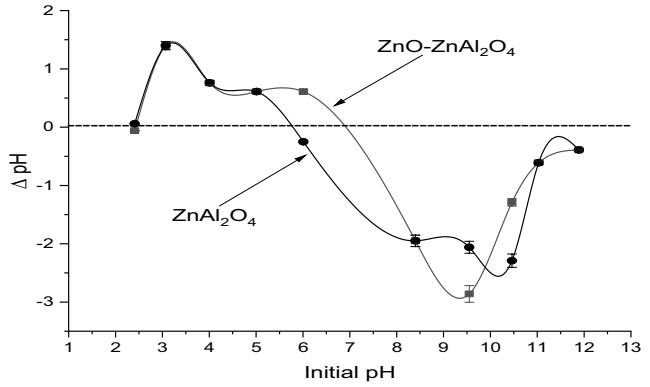

Fig. 5. Determination of the pH of the zero point of charge "pH_{pzc}" on the $ZnAl_2O_4$ and $ZnO\text{-}ZnAl_2O_4$ (C_0 = 100 mg/L, T = 25°C, Va = 250 rpm).

more negatively charged sites existed on the surface of adsorbent at higher pH, which is adverse for the adsorption of MO due to electrostatic repulsion. On the other hand, there are more OH^- ions that compete with anionic dye for the finite adsorption sites in the alkaline aqueous solution [25].

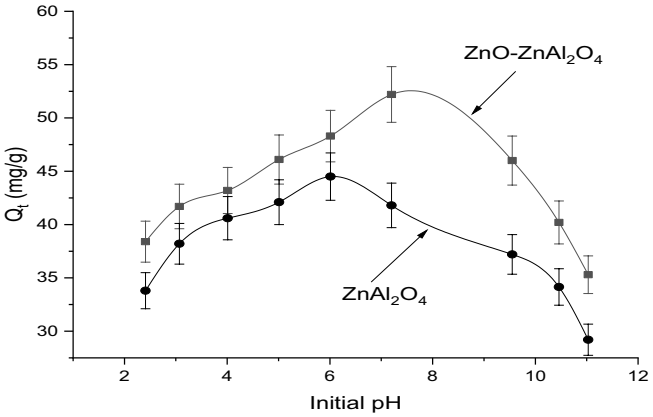

Fig. 6. Effect of pH on the adsorption of methyl orange on $ZnAl_2O_4$ and $ZnO\text{-}ZnAl_2O_4$ (C_0 = 100 mg/L, adsorbent mass = 50 mg, T = 25°C and Va = 250 rpm).

3.7.2. Effect of contact time and initial methyl orange concentration

Fig. 7a and b represent the adsorption quantities of MO for the two adsorbents at various initial methyl orange concentrations 10–150 mg/L at a temperature of 25°C, pH = 6.2 and with an adsorbent dosage of 50 mg. The results obtained show that the adsorption capacity of the dye increases with the increase in the initial concentration of MO, for the two adsorbents.

This is due to the high driving force to overcome the resistance to the mass transfer of dye between aqueous and the solid phase. Therefore, a higher initial concentration of dye will enhance the adsorption process, this agrees with Hanoon et al. [26] and Yang et al. [27].

3.7.3. Effect of the amount of adsorbent

The mass of adsorbent is an essential parameter in adsorption studies because it determines the capacity of the adsorbent for a given initial concentration of adsorbate solution.

The results about the effect of dosage on adsorption are described in Fig. 8.

The results showed that the adsorption quantities of MO decreases from 52.2% to 18.6% and from 44.5% to 13.7% with increasing adsorbent dosage from 50 to 300 mg for $ZnO\text{-}ZnAl_2O_4$ and $ZnAl_2O_4$, respectively. This can be explained by the formation of excessive active sites on $ZnO\text{-}ZnAl_2O_4$ and $ZnAl_2O_4$ at higher adsorbent dosage, which leads to many vacant sites, while the number of adsorbate molecules remains constant. Considering the economic and adsorption performance aspects, 50 mg of adsorbent would be practical for an application as an optimal dosage [28].

3.8. Adsorption isotherms

In general, adsorption isotherms provide information on adsorbent enhancement, description of affinity and binding energy between adsorbate and adsorbent, and adsorption capacity [29]. Several adsorption isotherms are often used in the literature such as: Langmuir and Freundlich [30].

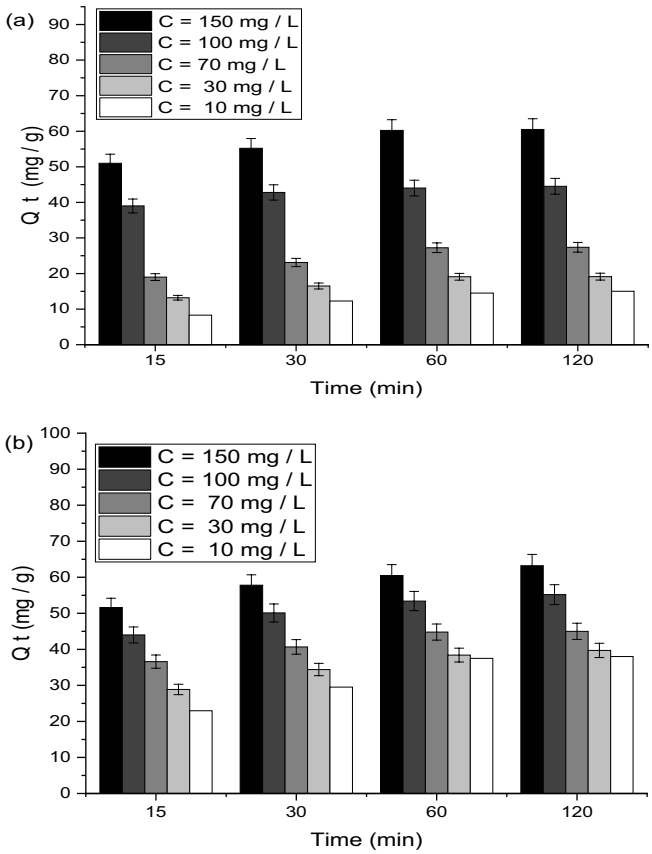

Fig. 7. Effect of the initial concentration of methyl orange and the contact time on the adsorption of methyl orange on: (a) $ZnAl_2O_4$ and (b) ZnO-$ZnAl_2O_4$ (adsorbent mass = 50 mg, T = 25°C, pH = 6.2 and Va = 250 rpm).

The Langmuir model is the most widely used model to describe the adsorption process, it suggests monolayer adsorption on a surface with a finite number of identical sites. It is expressed by Eq. (2):

$$\frac{1}{Q_e} = \frac{1}{Q_m} + \frac{1}{Q_m \times K_L \times C_e} \tag{2}$$

where C_e (mg/L) denotes the concentration of adsorbate at adsorption equilibrium, Q_e (mg/g) is the adsorption capacity, Q_m (mg/g) is the maximum adsorption capacity, and K_L (L/mg) is the Langmuir adsorption constant.

The applicability of an adsorption can still be defined from a dimensionless constant called the separation factor or equilibrium parameter R_L Eq. (3) [31].

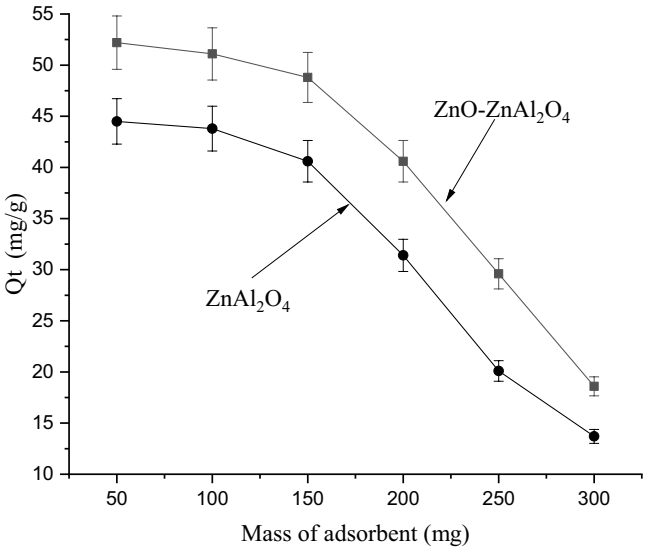

Fig. 8. Effect of adsorbent mass on the adsorption of methyl orange on $ZnAl_2O_4$, and ZnO-$ZnAl_2O_4$ (C_0 = 100 mg/L, T = 25°C, pH = 6.2 and Va = 250 rpm).

$$R_L = \frac{1}{\left(1 + K_L \times C_0\right)} \tag{3}$$

$R_L > 1$ the adsorption conditions are unfavorable; $R_L < 1$ the adsorption conditions are favorable; $R_L = 0$ adsorption is irreversible.

The Freundlich model assumes that adsorption occurs on heterogeneous surfaces with formation of more than one adsorption monolayer on the surface with possible interactions between the adsorbed molecules [32].

The linear form of the Freundlich isotherm can be expressed as:

$$\ln\left(Q_e\right) = \frac{1}{n}\ln\left(C_e\right) + \ln\left(K_f\right) \tag{4}$$

where K_f (mg/g) is the Freundlich adsorption constant and n is a constant depending on the nature of the adsorbate and the temperature.

For low values of n ($0.1 < n < 0.5$) the adsorption is good, while the highest values reveal moderate ($0.5 < n < 1$) or weak ($n > 1$) adsorption [32].

In our study, the linear plots of these isotherm models are illustrated in Fig. S1 for the adsorbents $ZnAl_2O_4$ and ZnO-$ZnAl_2O_4$ for comparison purposes and all of their coefficients are listed in Table 3.

Table 3
Adsorption isotherm parameters of methyl orange on $ZnAl_2O_4$ and ZnO-$ZnAl_2O_4$

Adsorbents	Langmuir model				Freundlich model		
	K_L (L/g)	Q_m (mg/g)	R^2	R_L	n	K_f (mg^{1-n}·L^n)/g	R^2
$ZnAl_2O_4$	0.217	46.24	0.9842	0.0468	3.12	10.571	0.9513
ZnO-$ZnAl_2O_4$	0.174	62.85	0.9920	0.0543	2.85	13.136	0.9677

In the light of these results, we can conclude that the Langmuir model seems the most appropriate to describe the phenomenon of fixation of MO ions on the two adsorbents, this with regard to the values of the higher correlation coefficients and close to 1 (0.9920 for ZnO-$ZnAl_2O_4$ and 0.9842 for $ZnAl_2O_4$ and the R_L values ($0 < R_L < 1$). The maximum adsorption capacity calculated for ZnO-$ZnAl_2O_4$ is equal to 62.85 mg/g higher than that calculated for $ZnAl_2O_4$, this leads to say that ZnO-$ZnAl_2O_4$ has the highest ability to remove MO molecules.

3.9. Adsorption kinetics

There are several kinetic models to study the adsorption mechanism, in the present work, two kinetic models have been selected namely the pseudo-first-order kinetic model, the pseudo-second-order kinetic model and intraparticle diffusion model [33]. The linear forms of kinetic models:

3.9.1. Pseudo-first-order kinetics model

This kinetic model assumes that the adsorption rate at a time "*t*" is proportional to the difference between the quantity adsorbed at equilibrium and that at time "*t*".

The pseudo-first-order equation can be expressed as:

$$\ln\left(Q_e - Q_t\right) = -K_1 t + \ln\left(Q_e\right) \tag{5}$$

where K_1 is the rate constant for pseudo-first-order.

3.9.2. Pseudo-second-order model

In the field of adsorption, the pseudo-second-order model is a model that is often used to describe the kinetics of adsorption processes. It suggests that the adsorption mechanism involves chemisorption, which is a type of adsorption where there is a strong interaction between the adsorbate molecule and the solid adsorbent, including the exchange of electrons.

The pseudo-second-order equation can be expressed as:

$$\frac{t}{Q_t} = \frac{t}{Q_e} + \frac{1}{K_2 Q_e^2} \tag{6}$$

where K_2 is the rate constant for pseudo-second-order.

3.9.3. Intraparticle diffusion model

The intraparticle diffusion model, also known as the Weber and Morris model [34], is a mathematical representation used to understand and describe the diffusion mechanism involved in the process of adsorption. The model was proposed by Weber and Morris, and it aims to analyze the rate at which solute molecules or particles diffuse into the interior of adsorbent particles.

This model is represented by Eq. (7):

$$Q_t = K_i \times t^{0.5} + C \tag{7}$$

where Q_t (mg/g) represents the adsorption capacity at time *t*, *C* (mg/g) is the intercept which represents a constant related to the thickness of the boundary layer and K_i (mg/g·min$^{1/2}$) is the intraparticle rate constant.

The linear plots of these kinetic models are illustrated in Figs. S2 and S3 and all of their parameters are listed in Table 4.

The kinetic parameters determined from the experimental data of adsorption of MO on the two adsorbents indicate that the values of the correlation coefficient (R^2) for the second-order model present a better description of the kinetics of the adsorption reaction vs. the first-order model for all initial concentrations, intraparticle diffusion model and the process of the MO adsorption reaction. The pseudo-second-order rate constants decrease with increasing initial concentrations of MO. This implies that the competition to access the active sites of the adsorbents is greater for higher concentrations. Therefore, the adsorption rate will become lower.

In order to determine the diffusion coefficient for the reaction between MO and $ZnAl_2O_4$ and ZnO-$ZnAl_2O_4$ and assess whether adsorption is diffusion-controlled, we

Table 4
Kinetic parameters of methyl orange adsorption on $ZnAl_2O_4$ and ZnO-$ZnAl_2O_4$

Adsorbents	Initial concentration (mg/g)	Pseudo-first-order, pseudo-second-order parameters and intraparticle diffusion model									
		$K_1 \cdot 10^2$ (min^{-1})	$Q_{e,cal}$ (mg/g)	R^2	$K_2 \cdot 10^2$ (g/mg·min)	$Q_{e,cal}$ (mg/g)	R^2	K_i (mg/g·min$^{1/2}$)	C (mg/g)	R^2	$Q_{e,exp}$ (mg/g)
$ZnAl_2O_4$	150	10.50	29.06	0.764	3.56	48.53	0.999	5.05	19.54	0.601	46.33
	100	9.70	20,22	0.984	5.08	44.68	0.999	3.72	14.20	0.607	40.81
	70	8.30	15.35	0.863	5.78	27.78	0.999	2.30	8.58	0.619	36.37
	30	8.00	10.26	0.996	7.78	19.45	0.999	1.64	5.59	0.657	24.58
	10	6.60	10,80	0.677	9.82	10.27	0.997	0.90	2.25	0.760	10.03
ZnO-	150	10.60	47.94	0.986	0.284	68,49	0.999	5.70	21.30	0.618	68.05
$ZnAl_2O_4$	100	9.40	41.26	0.820	0.562	60.24	0.999	5.24	13.25	0771	59.21
	70	7.60	22.74	0.706	1.186	55.86	0.999	4.84	14.21	0.711	45.03
	30	6.50	21.24	0.736	2.695	39.37	0.999	3.25	12.25	0.613	39.72
	10	5.10	11.24	0.931	6.144	38.91	0.999	3.47	10.90	0.686	38.11

plotted the variation of the fixed quantities as a function of the square root of the time $Q_t = f(t^{1/2})$ for the two adsorbents (Fig. 9). The intraparticle diffusion model shows that the curve is composed of two separate linear parts [34,35]. The first is the step that controls the effect of the boundary layer, it is attributed to diffusion at the outer surface of the material. Once the latter is saturated, the particles of methyl orange penetrate the internal surface of the particles through the pores, this is the stage which corresponds to intraparticle diffusion. Previous studies have shown similar results in adsorption of Eriochrome and adsorption of textile [36].

3.10. Thermodynamic study

The equations mentioned below allowed us to determine the thermodynamic parameters at equilibrium characterizing the phenomenon and the strength of the adsorbate–adsorbent bonds, such as free energy change ($\Delta G°$), enthalpy ($\Delta H°$) and adsorption entropy ($\Delta S°$).

$$\Delta G° = -RT \times \ln\left(K_d\right) \tag{8}$$

The distribution coefficient "K_d" is calculated from the Eq. (9):

$$K_d = \frac{Q_e}{C_e} \tag{9}$$

The standard enthalpy "ΔH" and the standard entropy "ΔS" of adsorption can be determined from van't Hoff's equation:

$$\ln\left(K_d\right) = \frac{\Delta S°}{R} - \frac{\Delta H°}{RT} \tag{10}$$

where ΔG is the standard free energy change (kJ/mol), T is the temperature in Kelvin, R is the universal gas constant (8.314 mol/K), Q_e (mg/g), is equilibrium adsorption capacity, and C_e (mg/L) is the equilibrium concentration of dye.

The plot of $\ln(K_d)$ as a function of $1/T$ is shown in Fig. 10, and the thermodynamic parameter results obtained are grouped in Table 5. The positive values of the variation of the standard enthalpy $\Delta H°$ ($\Delta H° > 0$) confirm that the process of adsorption of MO on the two adsorbents is endothermic [38]. These values are less than 40 kJ/mol ($\Delta H° < 40$ kJ/mol). This implies that the adsorption process is reacted by a physical phenomenon (physisorption) in which the adsorbed MO molecules are bound by Van der Waals forces and electrostatic forces of attraction–repulsion of small energies. Negative values of $\Delta G°$ at different temperatures indicate the spontaneous nature of the adsorption process. The decrease in $\Delta G°$ with increasing temperature shows that adsorption is more favorable at low temperature. The negative value of $\Delta S°$ indicates that there is a decrease in disorder in the solid/solute interface solution system during the adsorption process [37].

3.11. Study after adsorption

To explain the mechanism of interaction between the groups responsible for the adsorption and the dyes, we

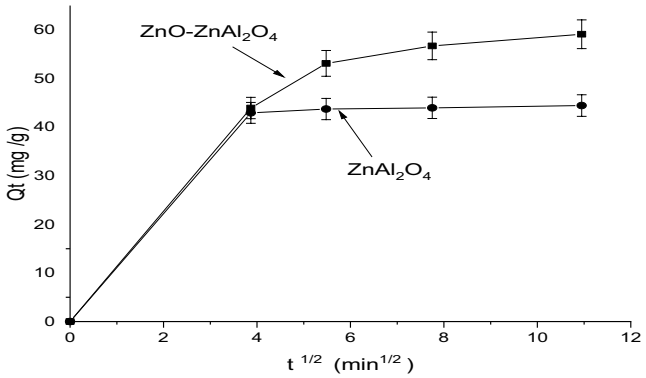

Fig. 9. Intraparticle diffusion for the adsorption of methyl orange, $ZnAl_2O_4$ and ZnO-$ZnAl_2O_4$ (C_0 = 100 mg/L, adsorbent mass = 50 mg, T = 25°C, pH = 6.2 and Va = 250 rpm).

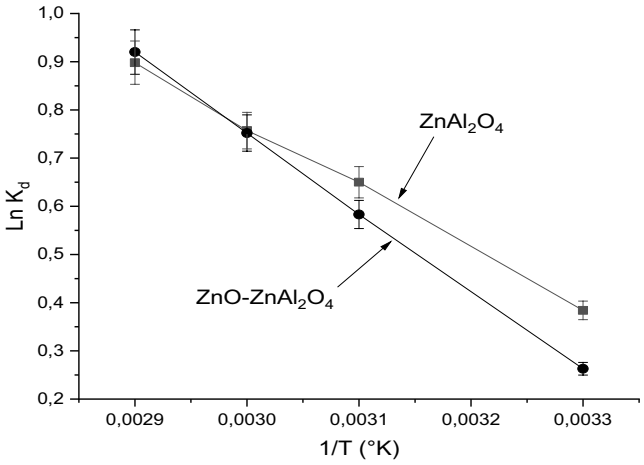

Fig. 10. Plot $\ln K_d$ as a function of $1/T$ for $ZnAl_2O_4$ and ZnO-$ZnAl_2O_4$ (C_0 = 100 mg/L, adsorbent mass = 50 mg, pH = 6.2 and Va = 250 rpm).

Table 5
Thermodynamic parameters of methyl orange adsorption

Temperature (°C)	$ZnAl_2O_4$			ZnO-$ZnAl_2O_4$		
	ΔG (kJ/mol)	ΔH (kJ/mol)	ΔS (kJ/mol)	ΔG (kJ/mol)	ΔH (kJ/mol)	ΔS (kJ/mol)
25	–0.754	10.57	0.038	–0.356	13.65	0.047
40	–1.324			–1.061		
50	–1.704			–1.531		
70	–2.464			–2.471		

analyzed catalysts by FTIR and SEM technique before and after the MO adsorption (Figs. 11 and 12). The FTIR spectra of catalysts before and after adsorption are shown in Fig. 11. Some new bands appeared on ZnO-$ZnAl_2O_4$ spectrum after the adsorption of MO. The bands at 1,629; 892; 1,313.7 and 1,115 cm^{-1} were attributed to –C=C, –C–H, the –C=N and –S=O, respectively, according to the literature [38,39]. In this work, the –C=N band was observed at 1,387 cm^{-1} (Fig. 11b). The bands observed at 1,655 cm^{-1} indicate the presence of the vibration of C=C stretching in phenyl groups of MO [39,40]. Stretching modes of –S=O are observed at 1,045 cm^{-1}, –C–H bending was observed at 890 cm^{-1} and $–CH_3$ vibrations was observed at 1,530 cm^{-1} [40].

SEM images of ZnO-$ZnAl_2O_4$ before and after adsorption show an almost ordered and highly porous lamellar structure with fine particles (Fig. 12a). After adsorption, it was observed that the surface was covered with the MO (Fig. 12b), which presents a morphology in the form of clusters of irregular fine shiny aggregates distributed in a random manner. These observations clearly indicate the presence of MO in the surface of ZnO-$ZnAl_2O_4$.

3.12. Suggested mechanism

The proposed mechanism suggests that methyl orange (MO) adsorption on a material composed of ZnO-$ZnAl_2O_4$ involves electrostatic interactions between MO and hydroxyl ions at adsorption sites on ZnO-$ZnAl_2O_4$ with a positive charge. Methyl orange (MO) contains a 3-amino group and a sulphonyl group, and the sulphonyl group is negatively charged due to its low pKa value. This negative charge makes MO an anionic dye. ZnO-$ZnAl_2O_4$ is the adsorption

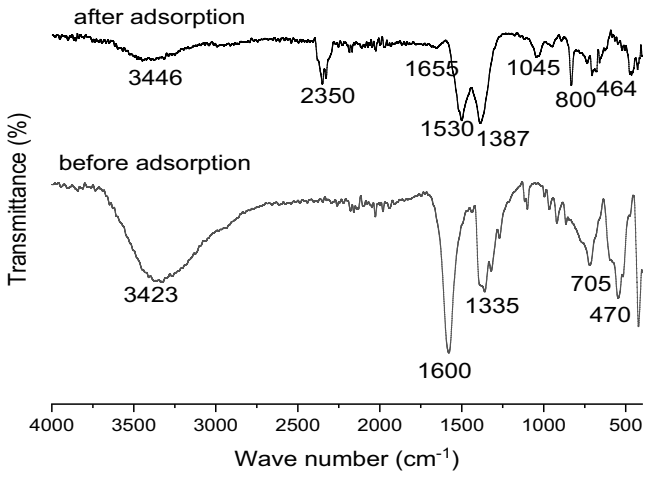

Fig. 11. Fourier-transform infrared spectra of ZnO-$ZnAl_2O_4$ (a) before adsorption and (b) after adsorption of methyl orange.

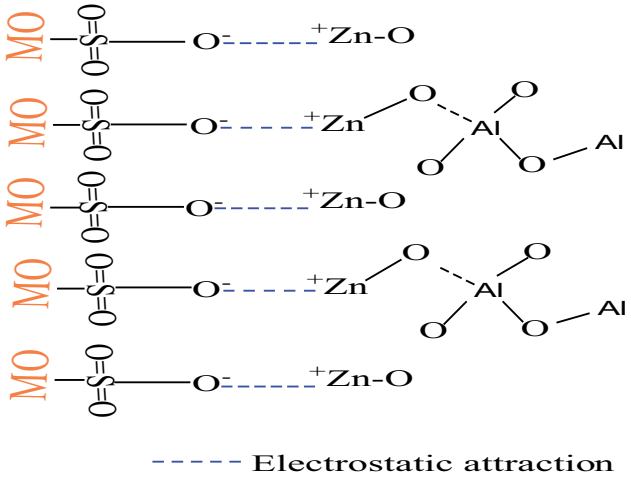

Fig. 13. Suggested mechanism of methyl orange removal by ZnO-$ZnAl_2O_4$.

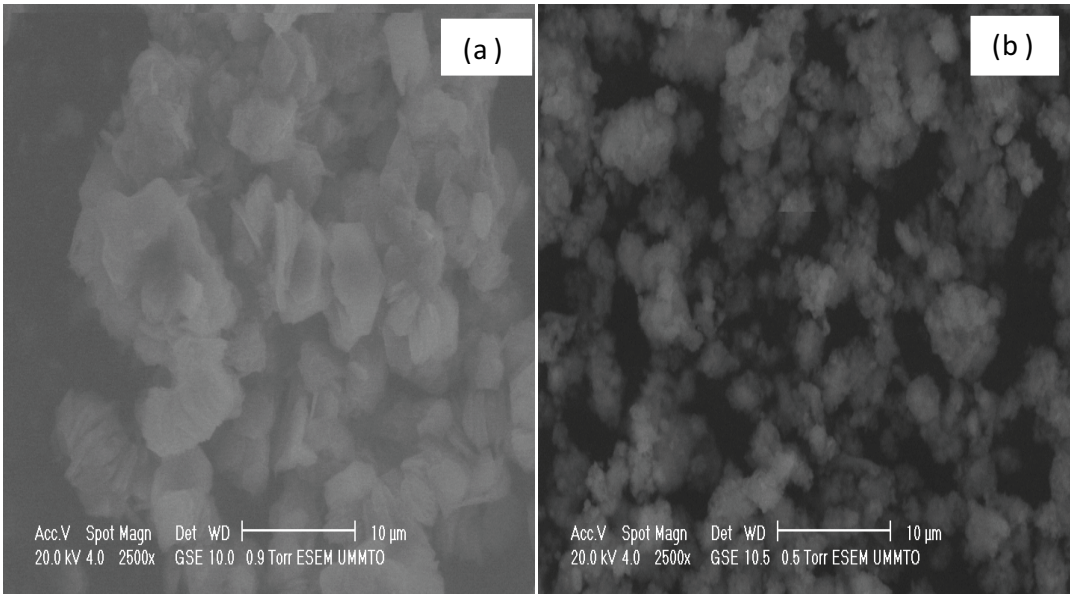

Fig. 12. Scanning electron microscopy images of ZnO-$ZnAl_2O_4$ (a) before adsorption and (b) after adsorption of methyl orange.

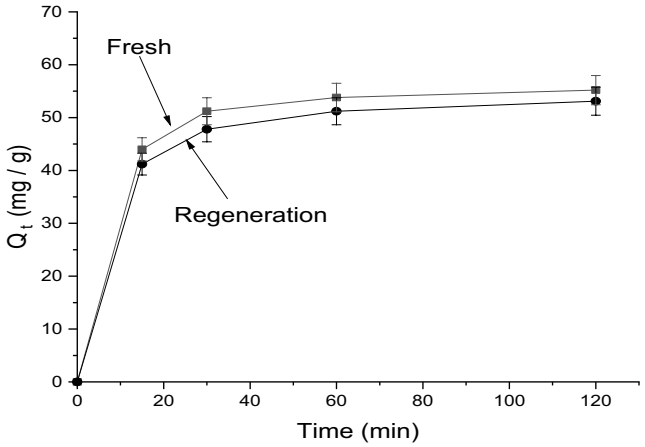

Fig. 14. Kinetic adsorption's comparison of methyl orange using a fresh and a regenerated ZnO-$ZnAl_2O_4$ (C_0 = 100 mg/L, adsorbent mass = 50 mg, T = 25°C, pH = 6.2 and Va = 250 rpm).

material, and it is suggested to have positive charge sites available for adsorption. When MO, which is negatively charged, comes into contact with the positively charged adsorption sites on ZnO-$ZnAl_2O_4$, electrostatic attractions occur. The hydroxyl ions present in the system can further facilitate the adsorption process. The mechanism suggests that MO interacts with hydroxyl ions, which may be present on the surface of ZnO-$ZnAl_2O_4$, and this interaction could aid in the adsorption of MO [41]. Overall, the proposed mechanism describes the electrostatic attraction between the negatively charged MO and positively charged adsorption sites on ZnO-$ZnAl_2O_4$, along with potential interactions with hydroxyl ions, may drive the adsorption of MO onto the material. This electrostatic interaction is a common phenomenon in adsorption processes and is frequently used to explain the adsorption of charged species on solid surfaces.

3.13. Regeneration of ZnO-$ZnAl_2O_4$

The regeneration of the ZnO-$ZnAl_2O_4$ adsorbent was carried out by washing with pure alcohol then agitated for 48 h. The solid obtained is filtered by centrifugation and washed with distilled water. After drying in an oven at 60°C overnight, the ZnO-$ZnAl_2O_4$ sample was reused for other adsorption tests. Fig. 14 shows the MO adsorption kinetics of fresh and the regenerated ZnO-$ZnAl_2O_4$. As can be seen, the regenerated adsorbent has an adsorption capacity almost similar to that of the fresh adsorbent.

This indicates that the regeneration process has been highly effective in restoring the adsorbent's functionality while minimizing waste and costs. When the regenerated adsorbent retains a capacity close to that of the fresh adsorbent, it suggests that the regeneration process successfully removed the adsorbed substances and restored the adsorbent's active sites.

4. Conclusion

The results obtained in this study suggest that hydrotalcite are very effective adsorbents for anionic dyes like methyl orange (MO). $ZnAl_2$ and Zn_2Al, were synthesized by co-precipitation method. The $ZnAl_2O_4$ and ZnO-$ZnAl_2O_4$ mixed oxides obtained after calcined of $ZnAl_2$ and Zn_2Al at 600°C, respectively. The samples were characterized by different physico-chemical techniques such as XRD, FTIR, BET method and SEM analysis.

The results obtained relating to the kinetics, thermodynamics and adsorption isotherms were used to clarify the mode of attachment of the dye to the adsorbent. We studied the capacity of elimination of MO in aqueous solution on our synthesized materials. The elimination was followed according to the reaction parameters such as: the initial pH of the solution, the mass of the adsorbent, the concentration of the adsorbate and the contact time. In this study, we obtained a neutral pH of the solution which can largely promote the adsorption of MO. We have deduced that the material ZnO-$ZnAl_2O_4$ has the greatest adsorption capacity compared to the material $ZnAl_2O_4$ due to its large specific surface area (155.07 m^2/g). The adsorption kinetics followed a pseudo-second-order kinetic model. The experimental equilibrium data were well fitted by the Langmuir isotherm model with the correlation coefficient greater than 0.9920. The thermodynamic parameters showed that the adsorption process was spontaneous and endothermic.

Acknowledgements

This work is supported by the Centre de Recherche Scientifiqueet Technique en Analyses Physico-Chimiques (CRAPC), Algeria, for the financial support.

References

[1] I. Manisalidis, E. Stavropoulou, A. Stavropoulos, E. Bezirtzoglou, Environmental and health impacts of air pollution: a review, Front. Public Health, 8 (2020) 14–27.
[2] R.R. Appannagari, Environmental pollution causes and consequences: a study, North Asian Int. Res. J. Social Sci. Humanit., 3 (2017) 151–161.
[3] S. Mitra, A.J. Chakraborty, A.M. Tareq, T.B. Emran, F. Nainu, A. Khusro, A.M. Idris, M.U. Khandaker, H. Osman, F.A. Alhumaydhi, J. Simal-Gandara, Impact of heavy metals on the environment and human health: novel therapeutic insights to counter the toxicity, J. King Saud Univ. Sci., 34 (2022) 101865, doi: 10.1016/j.jksus.2022.101865.
[4] F. Parvin, S. Islam, Z. Urmy, S. Ahmed, A.S. Islam, A study on the solutions of environment pollutions and worker's health problems caused by textile manufacturing operations, Biomed. J. Sci. Tech. Res., 28 (2020) 21831–21844.
[5] L.D. Ardila-Leal, R.A. Poutou-Piñales, A.M. Pedroza-Rodríguez, B.E. Quevedo-Hidalgo, A brief history of colour, the environmental impact of synthetic dyes and removal by using laccases, Molecules, 26 (2021) 3813, doi: 10.3390/molecules26133813.
[6] N.Y. Donkadokula, A.K. Kola, I. Naz, D. Saroj, A review on advanced physico-chemical and biological textile dye wastewater treatment techniques, Rev. Environ. Sci. Biotechnol., 19 (2020) 543–560.
[7] F. Touahra, S. Zemmache, S. Djema, R. Chebout, D. Lerari, K. Bachari, A new approach to the synthesis of $CuFe_2O_4$@CeO_2 direct Z-scheme with a core-shell structure for enhanced photo-degradation of methyl violet under ultraviolet and visible-light irradiation, Environ. Prog. Sustainable Energy, 41 (2022) e13865, doi: 10.1002/ep.13865.
[8] E.K. Radwan, H.H.A. Ghafar, A.S. Moursy, C.H. Langford, A.H. Bedair, G. Achari, Adsorptive removal of hazardous

organic water pollutants by humic acid–carbon hybrid materials: kinetics and isotherm study, Desal. Water Treat., 80 (2017) 297–305.
[9] P. Hu, L. Zhang, J. Wang, R. Huang, Removal of methyl orange from aqueous solution with crosslinked quaternized chitosan/bentonite composite, Desal. Water Treat., 80 (2017) 370–379.
[10] D. Chaillot, S. Bennici, J. Brendlé, Layered double hydroxides and LDH-derived materials in chosen environmental applications: a review, Environ. Sci. Pollut. Res., 28 (2021) 24375–24405.
[11] Z. Li, J. Zhang, C. Qu, Y. Tang, M. Slaný, Synthesis of Mg-Al hydrotalcite clay with high adsorption capacity, Materials, 14 (2021) 7231, doi: 10.3390/ma14237231.
[12] X. Liang, Y. Zang, Y. Xu, X. Tan, W. Hou, L. Wang, Y. Sun, Sorption of metal cations on layered double hydroxides, Colloids Surf., A, 433 (2013) 122–131.
[13] A. Machrouhi, N. Taoufik, A. Elhalil, H. Tounsadi, Z. Rais, N. Barka, Patent blue V dye adsorption by fresh and calcined Zn/Al LDH: effect of process parameters and experimental design optimization, J. Compos. Sci., 6 (2022) 115, doi: 10.3390/jcs6040115.
[14] A. El Khanchaoui, M. Sajieddine, M. Mansori, A. Essoumhi, Anionic dye adsorption on ZnAl hydrotalcite-type and regeneration studies based on "memory effect", Int. J. Environ. Anal. Chem., 102 (2022) 3542–3560.
[15] P.N. Patil, D.V. Sawant, R.N. Deshmukh, Physico-chemical parameters for testing of water - a review, Int. J. Environ. Sci., 3 (2012) 1194–1207.
[16] B. Djebarri, N. Aider, F. Touahra, R. Chebout, D. Lerari, K. Bachari, D. Halliche, Synergistic effect of bimetallic Ni-based catalysts derived from hydrotalcite on stability and coke resistance for dry reforming of methane, Chem. Afr., (2023), doi: 10.1007/s42250-023-00772-7.
[17] A.A. Alghamdi, A.-B. Al-Odayni, W.S. Saeed, A. Al-Kahtani, F.A. Alharthi, T. Aouak, Efficient adsorption of lead(II) from aqueous phase solutions using polypyrrole-based activated carbon, Materials, 12 (2019) 2020, doi: 10.3390/ma12122020.
[18] E.S. Zhitova, H. Chris Greenwell, M.G. Krzhizhanovskaya, D.C. Apperley, I.V. Pekov, V.N. Yakovenchuk, Thermal evolution of natural layered double hydroxides: insight from quintinite, hydrotalcite, stichtite, and iowaite as reference samples for Co_3^- and Cl-members of the hydrotalcite supergroup, Minerals, 10 (2020) 961, doi: 10.3390/min10110961.
[19] Z. Meng, F. Lv, X. Li, Q. Zhang, P.K. Chu, S. Komarneni, Y. Zhang, Simultaneous arsenate and alkali removal from alkaline wastewater by *in-situ* formation of Zn–Al layered double hydroxide, Microporous Mesoporous Mater., 227 (2016) 137–143.
[20] M.A. González, R. Trócoli, I. Pavlovic, C. Barriga, F. La Mantia, Capturing Cd(II) and Pb(II) from contaminated water sources by electro-deposition on hydrotalcite-like compounds, Phys. Chem. Chem. Phys., 18 (2016) 1838–1845.
[21] Z. Yu, D. Chen, M. Rønning, T. Vrålstad, E. Ochoa-Fernández, A. Holmen, Large-scale synthesis of carbon nanofibers on Ni–Fe–Al hydrotalcite derived catalysts: I. Preparation and characterization of the Ni–Fe–Al hydrotalcites and their derived catalysts, Appl. Catal., A, 338 (2008) 136–146.
[22] X. Yan, Z. Tian, W. Peng, J. Zhang, Y. Tong, J. Li, D. Sun, H. Ge, J. Zhang, Synthesis of nano-octahedral MgO via a solvothermal-solid-decomposition method for the removal of methyl orange from aqueous solutions, RSC Adv., 10 (2020) 10681–10688.
[23] M. Tangarfa, N.S.A. Hassani, Experimental Study of Tannic Acid Adsorption on Fluorite Surface: Particle Size Effect and Isotherm Modelling, 2022 2nd International Conference on Innovative Research in Applied Science, Engineering and Technology (IRASET), IEEE, Meknes, Morocco 2022.
[24] C.L. Qiao, Y.M. Xu, Y. Yin, Y.X. Xu, Y.H. Xiao, C.Q. Liu, Adsorption of methyl orange on ZnO supported by seawater-modified red mud, Water Sci. Technol., 85 (2022) 2208–2224.
[25] A.K. Cordova Estrada, F. Cordova Lozano, R.A. Lara Díaz, Thermodynamics and kinetic studies for the adsorption process of methyl orange by magnetic activated carbons, Air Soil Water Res., 14 (2021) 1–11, doi: 10.1177/11786221211013336.
[26] M.A. Hanoon, M.J. Ahmed, Adsorption of methyl orange from wastewater by using biochar, Iraqi J. Chem. Pet. Eng., 20 (2019) 23–29.
[27] K. Yang, L.G. Yan, Y.M. Yang, S.J. Yu, R.R. Shan, H.Q. Yu, B.C. Zhu, B. Du, Adsorptive removal of phosphate by Mg-Al and Zn-Al layered double hydroxides: kinetics, isotherms and mechanisms, Sep. Purif. Technol., 124 (2014) 36–42.
[28] Y. Raji, A. Nadi, M. Rouway, S. Jamoudi Sbai, W. Yassine, A. Elmahbouby, O. Cherkaoui, S. Zyade, Efficient adsorption of methyl orange on nanoporous carbon from agricultural wastes: characterization, kinetics, thermodynamics, regeneration and adsorption mechanism, J. Compos. Sci., 6 (2022) 385, doi: 10.3390/jcs6120385.
[29] M. Gouamid, M.R. Ouahrani, M.B. Bensaci, Adsorption equilibrium, kinetics and thermodynamics of methylene blue from aqueous solutions using date palm leaves, Energy Procedia, 36 (2013) 898–907.
[30] D. Balarak, J. Jaafari, G. Hassani, Y. Mahdavi, I. Tyagi, S. Agarwal, V.K. Gupta, The use of low-cost adsorbent (*Canola residues*) for the adsorption of methylene blue from aqueous solution: isotherm, kinetic and thermodynamic studies, Colloids Interface Sci. Commun., 7 (2015) 16–19.
[31] D. Humelnicu, I. Zinicovscaia, I. Humelnicu, M. Ignat, N. Yushin, D. Grozdov, Study on the SBA-15 silica and ETS-10 titanosilicate as efficient adsorbents for Cu(II) removal from aqueous solution, Water, 14 (2022) 857–862.
[32] S. Kalam, S.A. Abu-Khamsin, M.S. Kamal, S. Patil, Surfactant adsorption isotherms: a review, ACS Omega, 6 (2021) 32342–32348.
[33] L.M. Silva, M.J. Muñoz-Peña, J.R. Domínguez-Vargas, T. González, E.M. Cuerda-Correa, Kinetic and equilibrium adsorption parameters estimation based on a heterogeneous intraparticle diffusion model, Surf. Interfaces, 22 (2021) 100791–100800.
[34] S. Karmaker, F. Sintaha, T.K. Saha, Kinetics, isotherm and thermodynamic studies of the adsorption of Reactive Red 239 dye from aqueous solution by chitosan 8B, Adv. Biol. Chem., 9 (2019), doi: 10.4236/abc.2019.91001.
[35] M.V. Maslova, V.I. Ivanenko, N.Yu. Yanicheva, N.V. Mudruk, Comparison of the sorption kinetics of lead(II) and zinc(II) on titanium phosphate ion-exchanger, Int. J. Mol. Sci., 21 (2020) 447, doi: 10.3390/ijms21020447.
[36] P. Haller, I. Machado, J. Torres, A. Vila, N. Veiga, Fe(III)-complex-imprinted polymers for the green oxidative degradation of the methyl orange dye pollutant, Polymers, 13 (2021) 3127, doi: 10.3390/polym13183127.
[37] A. Kali, A. Amar, I. Loulidi, C. Hadey, M. Jabri, A.A. Alrashdi, H. Lgaz, M. Sadoq, A. El-Kordy, F. Boukhlifi, Efficient adsorption removal of an anionic azo dye by lignocellulosic waste material and sludge recycling into combustible briquettes, Colloids Interfaces, 6 (2022) 22, doi: 10.3390/colloids6020022.
[38] X. Wang, J. Baker, K. Carlson, Z. Li, Mechanisms of selected anionic dye removal by clinoptilolite, Crystals, 12 (2022) 727, doi: 10.3390/cryst12050727.
[39] R. Nandini, B. Vishalakshi, A study of interaction of methyl orange with some polycations, E-J. Chem., 9 (2012) 343928, doi: 10.1155/2012/343928.
[40] B. Grégoire, J.L. Bantignies, R. Le-Parc, B. Prélot, J. Zajac, G. Layrac, D. Tichit, G. Martin-Gassin, Multiscale mechanistic study of the adsorption of methyl orange on the external surface of layered double hydroxide, J. Phys. Chem. C, 123 (2019) 22212–22220.
[41] R. Kumar, G. Kumar, A. Umar, Zinc oxide nanomaterials for photocatalytic degradation of methyl orange: a review, Nanosci. Nanotechnol. Lett., 6 (2014) 631–650.

Supporting information

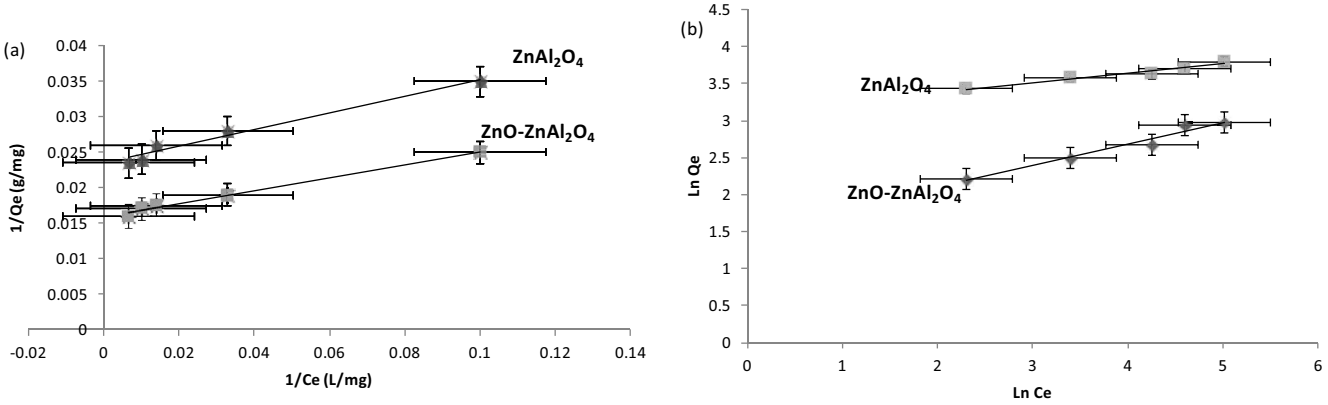

Fig. S1. (a) Langmuir isotherms and (b) Freundlich isotherms for the adsorption of methyl orange on $ZnAl_2O_4$ and ZnO-$ZnAl_2O_4$ (C_0 = 10–150 mg/L, adsorbent mass = 50 mg, T = 25°C, pH = 6.2 and Va = 250 rpm.

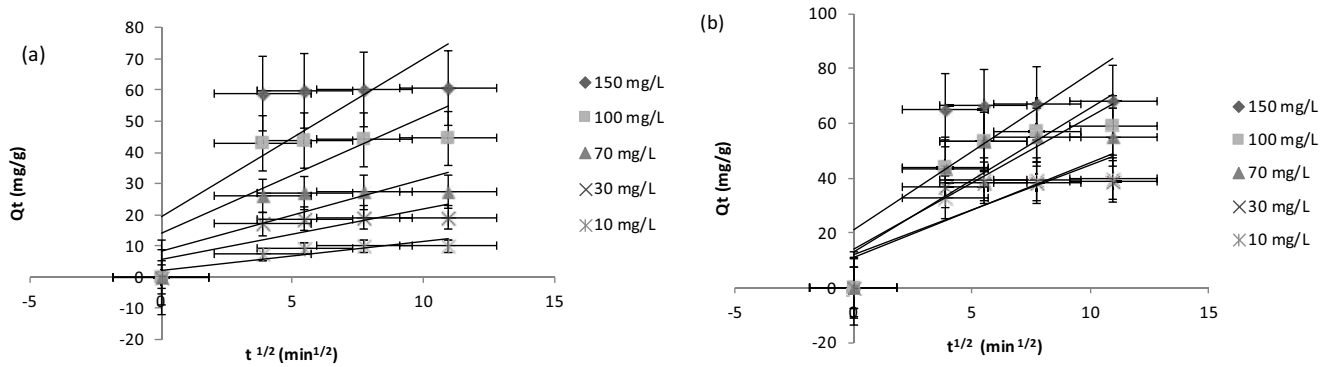

Fig. S2. Pseudo-first-order kinetics for the adsorption of methyl orange on: (a) $ZnAl_2O_4$ and (b) ZnO-$ZnAl_2O_4$ (C_0 = 100 mg/L, adsorbent mass = 50 mg, T = 25°C, pH = 6.2 and Va = 250 rpm).

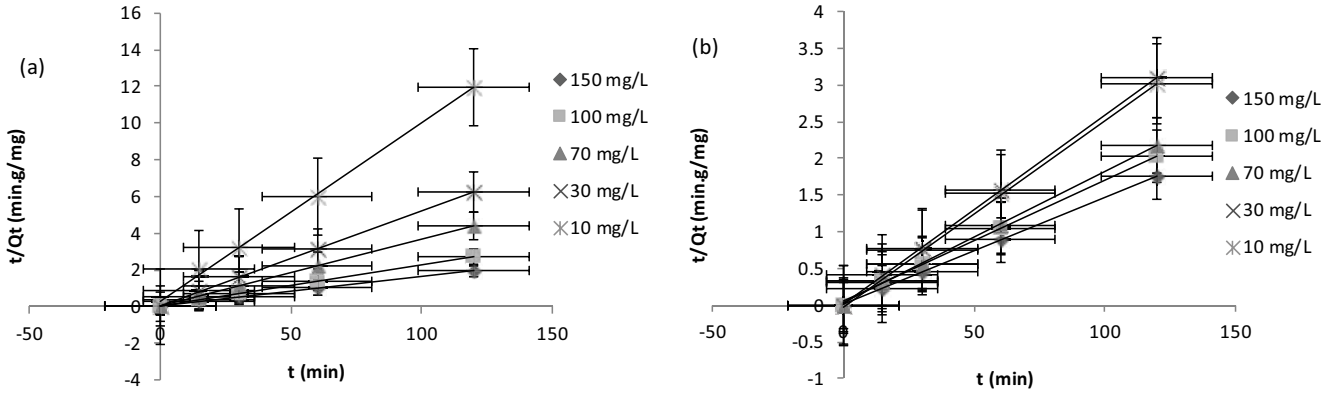

Fig. S3. Pseudo-second-order kinetics for adsorption of methyl orange on: (a) $ZnAl_2O_4$ and (b) ZnO-$ZnAl_2O_4$ (C_0 = 100 mg/L, adsorbent mass = 50 mg, T = 25°C, pH = 6.2 and Va = 250 rpm).